

Design and Experiments of Flexible Ultrasonic Motor Using a Coil Spring Slider

Kanada, Ayato

Department of Mechanical Engineering, Toyohashi University of Technology

Mashimo, Tomoaki

Department of Mechanical Engineering, Toyohashi University of Technology

<https://hdl.handle.net/2324/7172243>

出版情報 : IEEE/ASME Transactions on Mechatronics. 25 (1), pp.468-476, 2019-12-13. Institute of Electrical Electronics Engineers (IEEE)

バージョン :

権利関係 : © 2019 IEEE. Personal use of this material is permitted. Permission from IEEE must be obtained for all other uses, in any current or future media, including reprinting/republishing this material for advertising or promotional purposes, creating new collective works, for resale or redistribution to servers or lists, or reuse of any copyrighted component of this work in other works.



Design and Experiments of Flexible Ultrasonic Motor using a Coil Spring Slider

Ayato Kanada, *Student Member, IEEE*, and Tomoaki Mashimo, *Member, IEEE*

©2020 IEEE. Personal use of this material is permitted. Permission from IEEE must be obtained for all other uses, in any current or future media, including reprinting/republishing this material for advertising or promotional purposes, creating new collective works, for resale or redistribution to servers or lists, or reuse of any copyrighted component of this work in other works. DOI: 10.1109/TMECH.2019.2959614

Abstract—This paper proposes a flexible ultrasonic motor that consists of a single metal cube stator with a hole and an elastic elongated coil spring inserted into the hole. When voltages are applied to piezoelectric plates on the stator, the coil spring moves back and forward as a linear slider. The use of the coil spring brings flexibility for the motor and enables a long stroke to access to deeper sites. Furthermore, the coil spring provides an appropriate pre-pressure between the stator and the coil spring to enhance the motor output. We formulate the relation between the coil spring parameters and the pre-pressure to clarify the design methodology of the flexible ultrasonic motor. We model the linear motion of the coil spring by an equation of motion and compare it with the transient response by experiments. The flexible ultrasonic motor prototype achieved a translation at a speed of 120 mm/s and demonstrated a force of 0.45 N, and a stable motion even when the coil spring is being bent.

Index Terms—Ultrasonic motor, soft actuator, pre-pressure, coil spring, continuum robot.

I. INTRODUCTION

CONTINUUM robots that can access hard-to-reach targets in unpredictable environments have a wide range of potential applications from rescue to medicine [1]–[3]. For example, a typical place where continuum robots apply is the interior of gastrointestinal tracts which are soft and possess considerable curvatures. A flexible and elongated continuum robot goes inside our body via the mouth and enables the diagnosis and treatment of digestive diseases. With the increase in the expectation of such continuum robots, many hardware designs have been proposed and demonstrated. The important characteristics of these robots to explore deeper and inaccessible sites are flexibility and stroke. High flexibility is necessary to conform to surroundings and a long stroke expands reachable work areas. One challenge of continuum robot design is to have both high flexibility and long stroke in the elongated body with a small diameter (e.g., concentric tube robots [4]). However, it is difficult to have both the characteristics because the designable space inside the elongated tube robots is limited.

Typical driving methods for continuum robots are tendon-driven and pneumatically driven [5]–[7]. For example, tendon-driven robots are controlled by wires that are connected to electromagnetic motors or shape memory alloys [8]–[12]. These robots can obtain a relatively slender body and good accessibility into narrower spaces, but they require many complicated mechanical components. Pneumatically driven robots have an inherent compliance. There are several pneumatic actuators with a large stroke (e.g., origami structures [13] and folded balloons [14]), but they require a large and complex system using a compressor, air tubes, and valves at external sites.

Ultrasonic motors based on piezoelectric phenomena are known as the actuators used for the autofocus system in camera lenses [15]. None of us may have thought that these ultrasonic motors can be used as flexible actuators because they are in general known as rigid actuators without softness [16]–[19]. Before talking about the flexible ultrasonic motor that we propose, let us summarize several advantages of the existing ultrasonic motors. (i) The high torque density that generates a high torque from a small volume stator is a key characteristic to miniaturize the stator. (ii) The simple structure consisting of a stator and a rotor reduces the number of mechanical components. (iii) The design flexibility that can make the stator hollow is suited for applications in narrow spaces. (iv) They have an MRI compatibility [15] and might be useful for medical applications such as MRI compatible concentric tube robots. All these advantages are desired characteristics to design new continuum robots.

In this paper, we propose a flexible ultrasonic motor that uses an elastic elongated coil spring as a linear slider. This motor simply consists of a single cube stator with a through-hole and a coil spring inserted into the hole. The coil spring has a slightly larger diameter than the stator hole and contacts the inner surface of the stator. Not only does the coil spring provide flexibility to the slider, but also acts as a pre-pressure mechanism to improve motor output. When voltages are applied and the stator generates a driving force, the coil spring moves back and forth as shown in Fig. 1. This motor can obtain both a flexibility and stroke (travelling distance) by designing the dimensions of the coil spring. The flexibility is determined by coil spring parameters, such as the diameter, the cross-section dimensions, and Young's modulus. The travelling distance of the flexible spring slider can be designed to be

This work was supported by JSPS KAKENHI Grant Number 16H06075 and the Leading Graduate School Program 03.

A. Kanada and T. Mashimo are with the Department of Mechanical Engineering, Toyohashi University of Technology, 1-1 Hiragi-gaoka, Tempaku-cho, Toyohashi, Aichi, 441-8580, Japan e-mail: (see <http://eiiris.tut.ac.jp/mashimo/wordpress/en/top-page/>).

almost the same as the length of the coil spring.

The main contribution of this paper is the design and experimental characterization of the flexible ultrasonic motor. It reveals the relation of the motor performance to the pre-pressure determined by the coil spring dimensions. (The motion of a flexible ultrasonic motor was partially shown in a conference proceeding [20], but the design was not mentioned and the experiments were primitive.) The rest of the paper is organized as follows. In Section II, we describe the driving principle of the flexible ultrasonic motors and clarify how to formulate the relationship between the stator and the coil spring. Section III shows a prototype flexible ultrasonic motor and evaluates basic performance such as the thrust force and velocity in experiments. In Section IV, the linear motion of the coil spring presented in Section II is compared with the transient response experiment.

II. PRINCIPLE AND MODELING

A. Driving Principle

Fig. 2 shows the driving principle of the flexible ultrasonic motor for a linear motion. The stator is composed of a single metallic cube with a through hole and two piezoelectric plates adhered on the sides, as shown in Fig. 2(a). The piezoelectric plates are polarized in the thickness direction and their outside is positive pole. The negative pole bonded to the metallic cube is equivalent to ground. To move the coil spring slider linearly, two vibration modes are simultaneously excited by the piezoelectric plates as the driving principle. We call the two vibration modes T1 and T2 modes for translation. Fig. 2(b) shows how these vibration modes vibrate. The T1 mode is symmetric about the stator center, whereas the T2 mode is asymmetric. When two voltages are applied to the piezoelectric plates, both modes are excited at the same driving frequency. These two voltages are expressed as

$$E_1 = A_E \sin(2\pi f_E t) \quad (1)$$

$$E_2 = A_E \cos(2\pi f_E t) \quad (2)$$

where A_E and f_E are the amplitude and the frequency of the applied voltage, respectively. The frequency f_E is adjusted to be equal to the natural frequency of both vibration modes. When the symmetric and asymmetric modes are excited, the stator vibration describes an elliptical trajectories, as shown in Fig. 2(c). These elliptical motions generate throughout the stator hole, and they become the maximum at both ends of the stator. They move the coil spring slider inserted into the stator hole by a friction between the stator and the slider. This driving principle that uses both symmetric and asymmetric modes is similar to that used in linear ultrasonic motors [21], [22].

B. Design of the Coil Spring and Pre-pressure

In the flexible ultrasonic motor that uses the friction drive as the principle, the most important parameter for optimizing its output is the pre-pressure between the stator and slider. The magnitude of the pre-pressure can be designed from the dimensions of the coil spring and the diameter of the stator

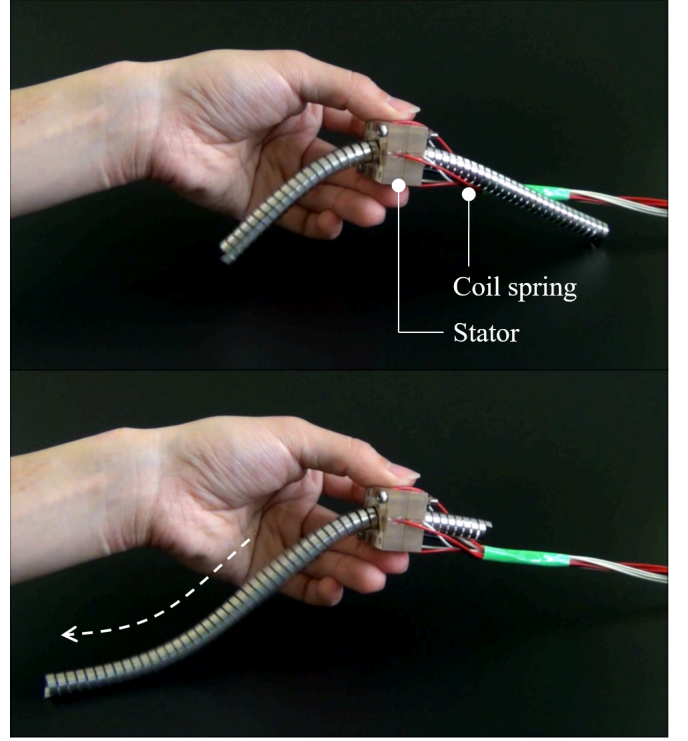


Fig. 1. Flexible ultrasonic motor. The coil spring inserted to the stator can move back and forth when voltages are applied.

hole. The coil spring slider is composed of a single metallic wire formed into a helix. It has a slightly larger diameter than the stator hole. Fig. 3(a) shows an original coil spring and the coil spring inserted to the stator hole. The coil spring with an outer radius r_1 shrinks to the hole radius r_2 . The shrinkage of the outer radius is defined as $\Delta r (= r_1 - r_2)$. The coil spring has a rectangular cross-section with a width b and a thickness h , as shown in the detailed view in Fig. 3(a). The median centerline of the coil spring exists at the cross-section center vertically, and the median centerline length that spirals inside the stator hole is defined as L . In other words, L is the product of 2π , the radius r_2 , and the number of turns N between both the edges of the stator after the coil insertion:

$$L = 2\pi r_2 N \quad (3)$$

When the coil spring is inserted into the stator hole, the shrunk coil generates the pre-pressure P at the interface between the stator and the coil spring as shown in the right of Fig. 3(a). To estimate the pre-pressure value from the coil's parameters, we consider two types of the elastic potential energy stored in the coil spring: strain energies by a shrinkage in the radial direction and by bending deformation. Assuming that these two energies take the same value, we can estimate the pre-pressure using this equivalence. First, we consider the energy by the shrinkage in the radial direction. Deriving a rigid solution of the radial deformation is too complicated because the coil spring with a thick cross-section has a non-linearity. In addition, the shrinkage of the coil spring results in the radial and circular deformations. To simplify this radial deformation, we regard the coil spring as a cylinder with an unknown

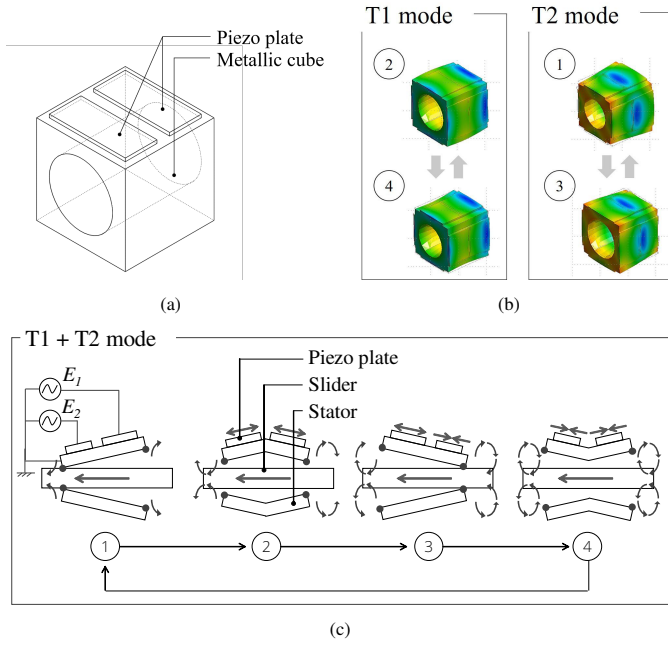


Fig. 2. The driving principle of the flexible ultrasonic motors. (a) Schematic of the stator. (b) Vibration modes (T1 and T2 modes) generated by the stator. (c) When T1 and T2 modes are simultaneously excited, the stator generates an elliptical motion and moves a slider.

elastic coefficient. When the pressure P is applied in the radial direction, the coil spring shrinks with a displacement of Δr . The work done by the pressure is equivalent to the strain energy stored in the coil spring:

$$U = \frac{1}{2} P b L \Delta r \quad (4)$$

where the product of the width b and length L is similar to the outer surface area where the pressure acts. This is the energy stored by the radial shrinkage, and the pressure P is still unknown in (4). The pressure P can be estimated after the strain energy is solved from the bending deformation.

Second, we consider the bending deformation of the Euler-Bernoulli beam, which is well known in the mechanics of materials [23]. Fig. 3(b) shows an element of the coil spring from the view of the axial direction of the stator hole. When the coil spring is inserted into the stator hole and bends, the upper part of the beam is in tension and the lower is in compression. In somewhere between the top and bottom, there is a neutral line, which is neither under tension nor compression. An elemental length of the neutral line that remains constant is defined as ds . Denoting the deformation at a distance y from the neutral line as Δds , the strain ε is determined as $\Delta ds/ds$ ($\varepsilon = \Delta ds/ds$). The strain energy by the bending deformation is the integral over the volume of the coil spring:

$$U = \int_V \frac{1}{2} E \varepsilon^2 dV = \frac{1}{2} E b L \int_{-h/2}^{h/2} \varepsilon^2 dy \quad (5)$$

where E is Young's modulus and the coil spring volume V is the product of b , h , and L . How the strain ε changes with y is geometrically determined when the dimensions of the coil

spring and the inner radius of the stator hole are determined. The strain ε is expressed as

$$\varepsilon = \frac{\Delta r}{r_1 r_2} y \quad (6)$$

Substituting (6) into (5), the strain energy can be obtained. Hence, these equations (4)-(6) show the relation between the pre-pressure and the design parameters of the coil spring slider. The pre-pressure P can be estimated by substituting the energy U solved in (5) into (4).

C. Modeling of Translational Motion

We build a mechanical model to estimate the linear motion of the flexible ultrasonic motor. In general, the motion of the ultrasonic motors is expressed as a first-order lag system regardless of rotary and linear motions [24]. When the stator generates a force F and the slider translates with the velocity \dot{x} , the motion is expressed as

$$m\ddot{x} + c\dot{x} = F \quad (7)$$

where m is the mass of the slider and c is the damping coefficient. This damping coefficient is determined by the axial velocity of the elliptical motion generated by the stator [25]. This is the simplest model of the linear ultrasonic motor with a rigid slider.

In the flexible ultrasonic motor, the coil spring exists at both sides of the stator; therefore, the equation of motion must incorporate the spring components of the coil spring in addition to the above model. Fig. 4 shows the model of the flexible ultrasonic motor with a coil spring slider, both the sides of which are expressed as mechanical components: m_L , c_L , and k_L are mass, damper, and spring at left side, respectively, and m_R , c_R , and k_R are those at right side. The sum of m_R and m_L is the mass of the whole coil spring slider. The terms with c_L and c_R are mechanical loss in the coil spring, regardless of the stator's vibration. This model has three degrees of freedom with x_L , x , and x_R . When the stator generate a force F , the motion of the coil spring can be expressed by the equation of motion:

$$\begin{bmatrix} m_L & 0 & 0 \\ 0 & 0 & 0 \\ 0 & 0 & m_R \end{bmatrix} \begin{bmatrix} \ddot{x}_L \\ \ddot{x} \\ \ddot{x}_R \end{bmatrix} + \begin{bmatrix} -c_L & c_L & 0 \\ -c_L & c_L + c_R & -c_R \\ 0 & c_R & -c_R \end{bmatrix} \begin{bmatrix} \dot{x}_L \\ \dot{x} \\ \dot{x}_R \end{bmatrix} + \begin{bmatrix} -k_L & k_L & 0 \\ -k_L & k_L + k_R & -k_R \\ 0 & k_R & -k_R \end{bmatrix} \begin{bmatrix} x_L \\ x \\ x_R \end{bmatrix} = \begin{bmatrix} 0 \\ F \\ 0 \end{bmatrix} \quad (8)$$

This three degrees of freedom model is usable at $x \cong 0$. i.e., the motion can be estimated when the displacement x is in the neighborhood of the stator position that generates a force F .

When the displacement x enlarges and the position that generates the force F is far from the stator ($x \gg 0$), the model (8) is not accorded to the actual. The stator is rigidly fixed in an experimental setup while the coil spring slider moves. In this case, the parameters of the coil spring slider change with the displacement x . Fig. 5 shows the right side of the stator when the displacement increases. Parameters at $x \gg 0$ are expressed using the prime symbol ($'$) to distinguish from

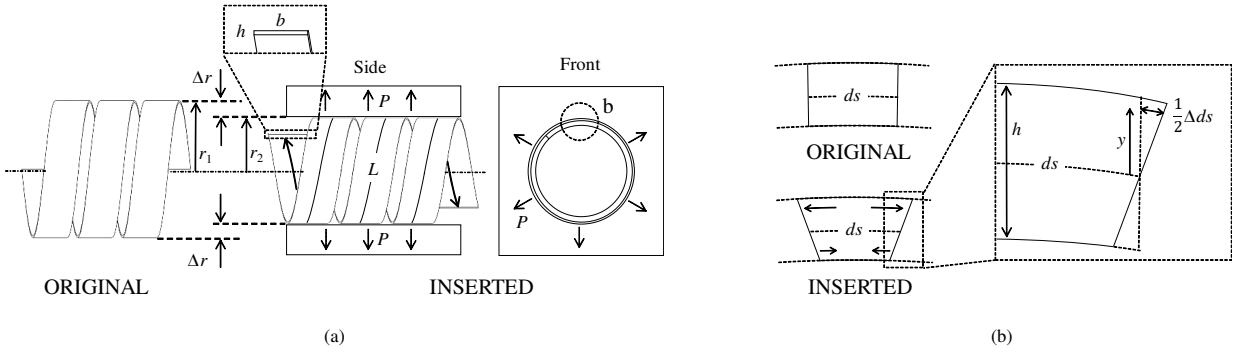


Fig. 3. Geometric relationship between the coil spring and the stator. (a) A coil spring with a slightly larger diameter than the stator hole diameter is inserted to the stator hole. The coil spring shrunk to the stator hole generates pre-pressure in the radial direction. (b) The detail of the deformation of a coil spring element. The cross section either lengthen or shorten, creating the strain.

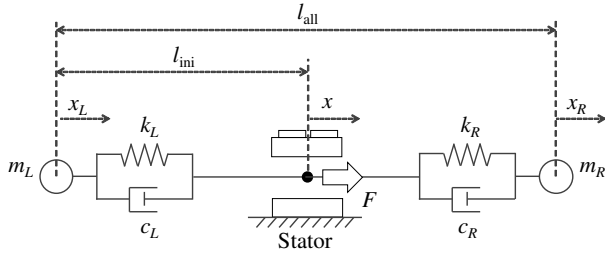


Fig. 4. A generalized model of the flexible ultrasonic motor, which is expressed as three-degrees of freedom system.

those of $x \gg 0$. The mass and the spring coefficient become a function of x . The mass m_R' is expressed as

$$m_R' = \frac{m}{l_{all}}(l_{ini} + x) \quad (9)$$

where m and l_{all} are the mass and length of the whole coil spring, respectively, l_{ini} is the initial length between the stator center and the coil spring end, defined in Fig. 4. The spring coefficient k_R' is

$$k_R' = 2l_{all} \frac{k}{l_{ini} + x} \quad (10)$$

where k is the spring constant of the whole coil spring. There is a damping coefficient, but it can be regarded as constant because its change is small. When the stator generates a force F , the displacement x occurs. Regarding that the behavior of the displacement x is independent of the motion of the masses, the displacement x can be simply estimated from the axial velocity of the elliptical motion. The relationship between displacements x and x_R' is expressed by the equation of motion with the variable mass and spring coefficient as follows.

$$m_R' \ddot{x}_R + c_R(\dot{x} - \dot{x}_R) + k_R'(x - x_R) = 0 \quad (11)$$

The motion at the left side in the model can be estimated by replacing index R with L in (9) to (11).

The natural angular frequency of the coil spring depends on length of the coil at both the sides of the stator. Seeing

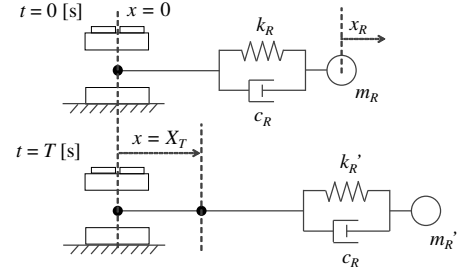


Fig. 5. A model at the right side of the coil spring. The mass and spring coefficient become variables of the displacement.

the right side from the stator, the natural angular frequency is described as

$$\omega = \sqrt{\frac{k_R'}{m_R'}} \quad (12)$$

This equation shows that the natural angular frequency decreases at larger displacements; that is, an end of the coil spring vibrates slowly as it moves away from the stator.

III. PERFORMANCE EVALUATION

A. Prototype of the Stator

We describe how to build the flexible ultrasonic motor. The stator consists of a metallic cube and four piezoelectric plates on its four sides. The cube, made of phosphor bronze, has a side length of 14 mm and a hole of 10 mm. Nickel plating is coated inside the hole to reduce wear. In the neighborhood of a corner of the stator, an internal thread of 1 mm in diameter is opened to connect to a ground line. Each piezoelectric plate with a length of 14 mm, a width of 10 mm, and a thickness of 0.5 mm, has two silver electrodes on one side. The four piezoelectric plates are bonded using an epoxy adhesive (TB2280E, ThreeBond, Japan) at 120 °C for 2 hours. Although the driving principle is explained by two piezoelectric plates in section II, more piezoelectric plates are used to supply larger electric power and to enhance motor output.

The resonances of the stator can be found by analyzing the frequency characteristics of admittance. To move the coil spring slider linearly, both the T1 and T2 modes should

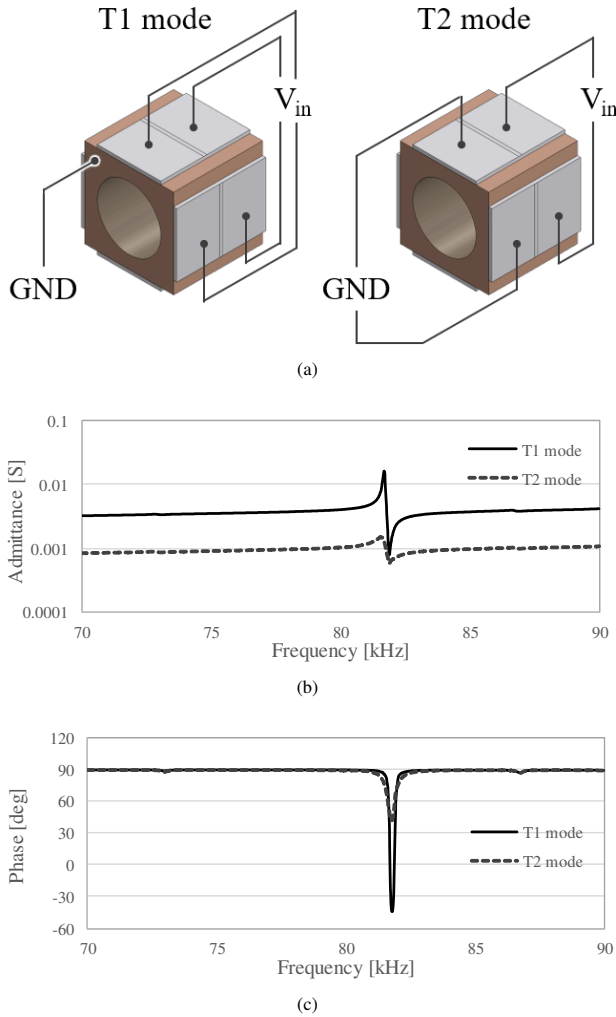


Fig. 6. Frequency response of the T1 and T2 modes. (a) Connection of the piezoelectric plates to the impedance analyzer. Frequency characteristic of (b) admittance and (c) phase. The result shows that T1 and T2 modes occur at the same resonant frequency.

be simultaneously excited at the same driving frequency. We confirm that the two vibration modes exist at the same frequency by observing the admittance curve. The admittance and phase of the stator are measured by an impedance analyzer (IM3570, Hioki E. E. Corp., Nagano, Japan). Changing the connection between the stator and the impedance analyzer can clarify the existence of both T1 and T2 modes. The left of Fig. 6(a) shows how to connect the piezoelectric plate electrodes to the analyzer. To excite T1 mode, the input voltage wire is connected to all eight electrodes of the piezoelectric plates, and the ground wire is connected to the metallic cube of the stator. When the voltage V_{in} is applied, all the piezoelectric plates repeat extension and contraction and generate T1 mode. On the other hand, to excite T2 mode, the input voltage is connected to the four electrodes at backward and the ground wire is connected to the other four electrodes at forward as shown in the right of Fig. 6(a). In this case, when the backward extends, the forward contracts, or vice versa. The repetition of these extension and contraction generates T2 mode.

Fig. 6(b) and (c) show the frequency response of the

admittance and phase, respectively, in which the solid lines and dashed lines show T1 and T2 modes, respectively. The resonance of T1 and T2 modes is observed as a steep change at almost the same frequency at around 82.0 kHz. These figures show that the T1 and T2 modes can be excited at the same driving frequency. When two voltages described in (1) and (2) are applied at 82.0 kHz, the excitation of T1 and T2 generate a translation as shown in Fig. 2 (c).

B. Relation between the Output and the Pre-pressure

The important characteristic of the proposed motor is how the motor output changes with respect to the pre-pressure. We experimentally clarify the relation of the pre-pressure with the thrust force and velocity generated by the motor. The coil spring model are given as a length $L = 94.2$ mm, width $b = 3$ mm, height (thickness) $h = 0.15$ mm, and Young's modulus $E = 196$ GPa. To change the pre-pressure, we insert several coil springs with different diameters ranging from 10 to 11 mm into the stator hole with a diameter of 10 mm. i.e., the coil spring with a larger diameter generates a large pre-pressure because the diameter of the stator hole is constant. The pre-pressure can be estimated from (4) after the strain energy is computed using (5). For example, when the coil spring diameter is 10 mm, the pre-pressure becomes zero. When a coil spring with a diameter of 11 mm is inserted into the stator hole, it generates a pre-pressure of $P = 0.036$ N/mm² and stores a strain energy of $U = 2.8$ mJ. (The strain energy is evaluated by the experiment shown in the Appendix).

In the experiments, the force is measured by a force gauge (ZP-20N, Imada Co., Japan) attached to the end of the coil spring. The velocity is measured by a laser displacement sensor (ZX2-LD50, OMRON Corp., Kyoto, Japan) placed in the travelling direction of the coil spring. In general, the velocity is calculated from the differentiation of the displacement, but estimating the motor velocity has large noise because the coil spring vibrates. We define the velocity from the displacement of the coil end after vibration and the period that the voltages apply. In this measurement, the transient time is ignored because the motor velocity peaks within a few milliseconds—the mass of the coil spring is much smaller than the output or brake force. During the experiments, the amplitude of the voltages is constant at $120 V_{p-p}$, and the frequency is adjusted to about 82 kHz to maximize the force and velocity. The optimum frequency has a slightly different value by coil springs because it depends on the pre-pressure value. For example, the optimum frequency at a coil diameter of 10.8 mm is 81.6 kHz, 0.2 kHz higher than the natural frequency at that of 10.15 mm.

Fig. 7 shows the behavior of the force and velocity when the pre-pressure varies. The force increases with the pre-pressure and peaks at 0.02 N/mm² (a coil diameter of 10.5 mm). A too large pre-pressure over 0.03 N/mm² (a coil diameter of 10.8 mm) decreases the force. On the other hand, the velocity is 200 mm/s at maximum, and decreases at higher pre-pressures. This is because a higher pre-pressure increases the friction at the stator-slider interface. Such a relation between the motor output and the pre-pressure has been seen in the preload

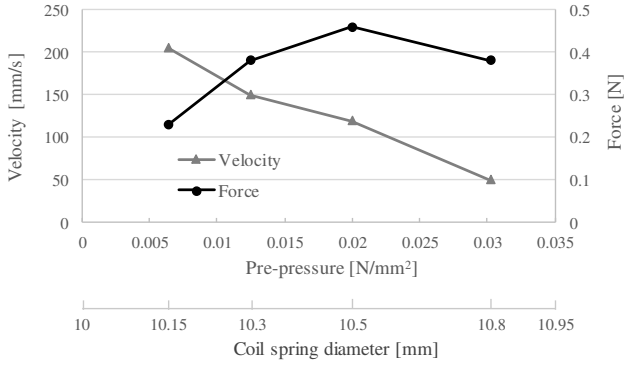


Fig. 7. Relation of the velocity and the force to pre-pressure. The pre-pressure is changed by using several coil springs with different diameters.

characteristic of ultrasonic motors with a friction drive [26], [27].

C. Load Characteristic

The relation between the force and velocity is a fundamental characteristic of linear actuators. It can be seen by measuring the motion of a coil spring that lifts load attached to its end. Fig. 8 shows an experimental setup to examine the force-velocity curve. The coil spring that generates an optimal pre-pressure of 0.02 N/mm² is placed in the setup vertically. External weights are connected to the coil spring as load. Because the weight of the coil spring is approximately 6 g, the sum of the coil spring and the additional weights is the force generated by the motor. The velocity is measured by the laser displacement sensor while the coil spring moves upward with the weights. Fig. 9 shows the force-velocity curve when the weights change from 0 to 50 g. The velocity decreases as the load increases, and the motor cannot generate a motion over a load of 50 g. This behavior is roughly linear as with the load characteristic of other ultrasonic motors [24].

D. Relation to the Bending Radius of the Coil Spring

Another important characteristic of the proposed motor is its flexibility. Evaluating the flexibility should be to examine the motion of the coil spring curved by constraints and/or external forces. The top of Fig. 10 shows the experimental setup to clarify how the velocity of the coil spring behaves under constraints. The coil spring end is fixed to a rotary constraint component that transfers the linear motion of the coil spring into a motion around an arc trajectory with a radius R . As shown in the bottom of Fig. 10, when the motor generates a linear motion, the coil spring moves to the left side of the stator and bends by the rotary constraint. The distance between the rotary constraint center and the coil spring end is equal to the bending radius R of the rotary constraint. The bending radius can be changed in the experimental setup. The laser displacement sensor installed at the right side measures another end of the coil spring that moves away from the sensor linearly.

Fig. 11 shows the relation between the bending radius and the velocity when the bending radius varies from 55 to 15

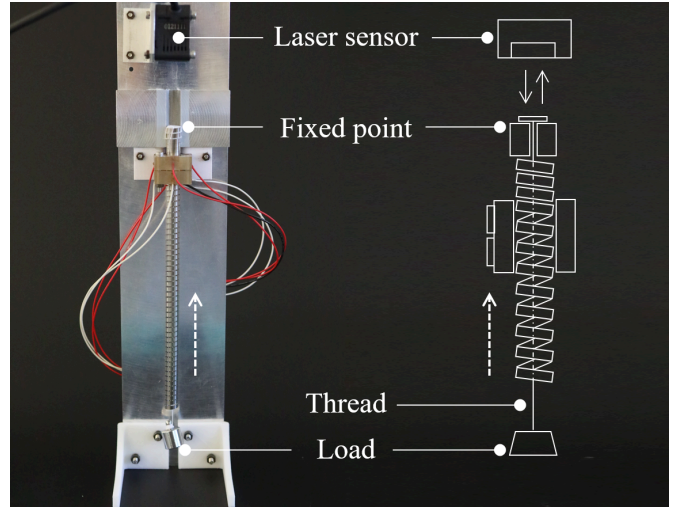


Fig. 8. Experimental setup for measuring the velocity when the flexible ultrasonic motor lifts a load. The coil spring slider moves upward in this experiment.

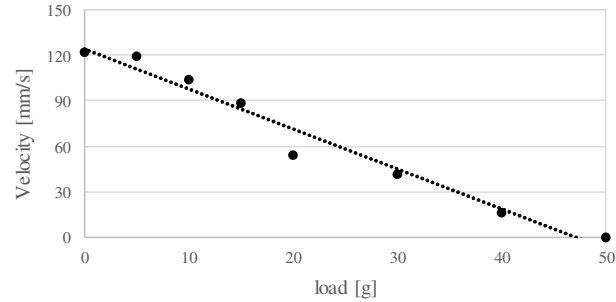


Fig. 9. Load characteristic of the flexible ultrasonic motor. It means a force-velocity curve.

mm. The result shows that the velocity is constant regardless of the bending radius—a smaller bending radius travels a shorter distance at less travelling time, and vice versa. This is because the velocity of the coil spring slider is determined by the steady-state vibration velocity of the stator in the friction drive [25]. Even at the smallest bending radius of 15 mm, the motor can generate an average translation velocity. The bending radius of 15 mm is close to the limit of bending because smaller bending radii are over the range of elastic deformation.

The flexibility of the coil spring slider can be designed by the material and dimensions of the coil spring. When the coil spring slider is very flexible by the design, it is difficult to transfer a force to the slider end, and buckling might occur. The coil spring slider with high stiffness can transfer a force, but it makes the pre-pressure unstable at smaller radii.

IV. DYNAMIC EVALUATION

A. Step Response

We measure the step response of the flexible ultrasonic motor to show the vibration of the coil spring and verify the dynamic model by experiments. The experimental setup is the same as that without the rotary constraint component shown

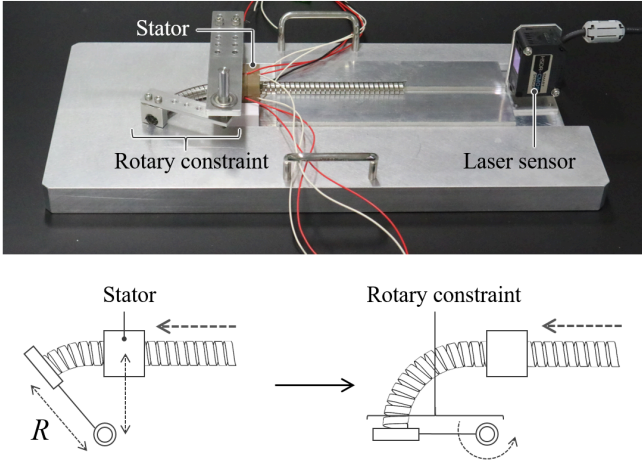


Fig. 10. Experimental setup to examine the relationship between the velocity and bending radius. The bending radius can be changed by the mechanical constraints.

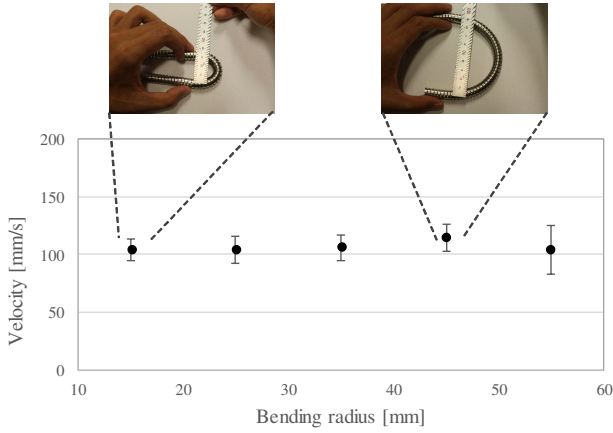


Fig. 11. The relationship between the velocity and bending radius (error bars indicate SD from 6 tests of one bending radius). The result shows that the velocity stays constant even if the coil spring is bent.

in Fig. 10. When the voltages are applied, the coil spring starts to move linearly. The displacement x with vibration is measured using the laser sensor. The vibration shown in the displacement x depends on the length of the coil spring, and the step responses are measured at the initial lengths l_{ini} of 40, 80, and 120 mm. The step responses are compared with the simulation. Assuming that the displacement x is independent of the vibration of the coil spring, the displacement x can be estimated from the coil spring's mass and the vibration velocity of the stator, as expressed in (7). The coil spring slider is supported by the experimental setup and is guided to move linearly, but a friction occurs by contact with the setup's base. A friction term $F_f = \mu m_R' g$ between the coil spring slider and the experimental setup is added in the left hand side of (11). When x is determined in (7), the motion of the coil spring end x_R' can be obtained in (11).

Fig. 12 shows the step responses when the control signal is on from time $t = 0$ to 50 ms. While the control signal is on, the voltages are applied to the motor from an external power

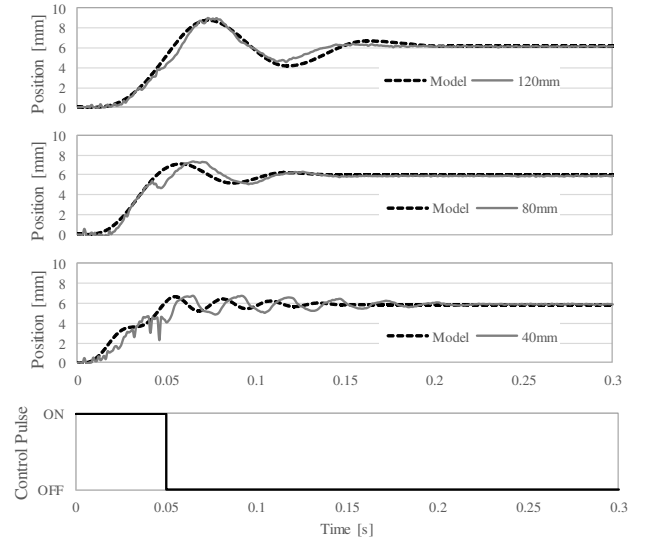


Fig. 12. Step response of the flexible ultrasonic motor when changing the initial length l_{ini} . The dashed and solid lines show the predicted result and the measured result, respectively.

TABLE I
MODEL PROPERTIES OF THE FLEXIBLE ULTRASONIC MOTOR

Symbol	Quantity	Value
m	Slider mass	0.006 kg
k	Spring constant	4.4 N/m
c	Damping coefficient	3.7 N·s/m
c_R	Damping coefficient	0.008 N·s/m
μ	Dynamic friction coefficient	0.24
l_{all}	Coil spring length	210 mm
F	Motor output	0.45 N

source. In all responses, when $t = 50$ ms, the driving force generated in the stator stops, but the coil spring still has an elastic energy. After the input signal is off, the vibration of the coil spring remains for 0.1–0.2 seconds. The experimental step response is compared with the simulations. The model parameters for simulation are given in Table I. The mass m , spring constant k and spring length l_{all} are determined from the design of the coil spring, and the damping coefficients c , c_R , and the friction coefficient μ are empirical. The motion of the coil spring is in agreement with the simulation. As the initial length l_{ini} shortens, the natural angular frequency increases as estimated in (11). This is because, at the short initial length, the mass m_R' reduces and spring constant k_R' enlarges. The natural angular frequencies of approximately 69, 100, and 201 rad/s, at the initial length l_{ini} of 120, 80, and 40 mm, respectively, are in agreement with the estimation.

V. CONCLUSION

In this paper, we demonstrated the first flexible ultrasonic motor using an elastic elongated coil spring. The proposed idea is the simplest way that provides a flexibility and a pre-pressure because there is no additional mechanism. The experiments showed the sufficient flexibility under a mechanical constraint and an accordance between the model and experiments. Although only one example of the flexible

ultrasonic motor is shown in this paper, the design strategy can be extended to the other designs for soft and flexible actuation technologies. In addition to the flexibility, this idea should be valuable as a simple pre-pressure mechanism for a rotary or linear motor with a rigid output shaft. Taking it into account that a typical advantage of ultrasonic motors is a high energy density, the pre-pressure mechanism has a potential to be miniaturized for narrow spaces, such as the inside of camera lenses and cell phones.

Our next step is the use of two or more flexible ultrasonic motors as a flexible and elongated continuum robot. Further investigation about contact problems at the stator-slider interface is important to generate a stable motion for controlling multiple flexible ultrasonic motors. Because the stator can generate a rotary motion [20], the combination of rotation and translation might be more attractive as a robotic application. The position sensors are required for control. We have started the study on the position sensor using the coils spring as a variable resistance. In this idea, when the coil spring moves, the position can be measured by reading the value of the variable resistance. It can provide a flexible sensor system into the motor without additional components. Another study about a further miniaturization of the flexible ultrasonic motor might be required for smaller diameter continuum robots. We have achieved an ultrasonic motor that can generate both rotary and linear motions by the stator with a cube of 3.5 mm [28]. This miniaturization technology might be applied to build a medical continuum robot with smaller diameter.

APPENDIX A

EXPERIMENTAL VERIFICATION OF THE STRAIN ENERGY

In (5), we estimated the strain energy of the coil spring by the model of the bending deformation of the Euler–Bernoulli beam. There is another computational method for the strain energy using the bending moment [23]. The advantage of using the bending moment is that shows the strain energy from the angular displacement by a simple experiment. In this section, we derive the strain energy using the bending moment and verify it experimentally. We consider the case that the coil spring inserted to the stator hole generates the pre-pressure P between the stator and coil (Fig. 3(a)). At this time, the bending moment M acts both the ends of the coil spring and makes the beam planes either lengthen or shorten, thereby creating strains. The bending moment is expressed by integrating the strains:

$$M = \int_A E \epsilon y dA \quad (A1)$$

where dA is the differential element of the beam area. In the Euler–Bernoulli beam, the bending moment M can be solved from a given angular displacement ϕ . This is expressed as

$$\phi = \frac{ML}{EI} \quad (A2)$$

ϕ can be geometrically determined by the parameters of the coil spring and the hole diameter. Using the relation between ϕ and M , the strain energy U_s is rewritten to

$$U_s = \frac{M^2 L}{2EI} \quad (A3)$$

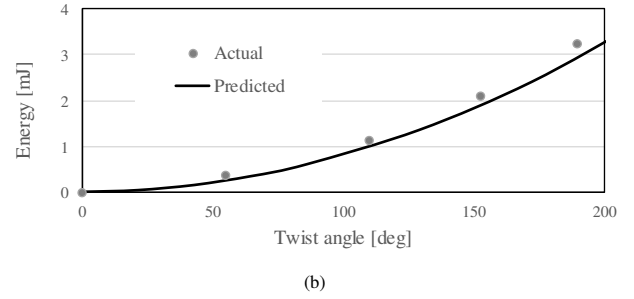
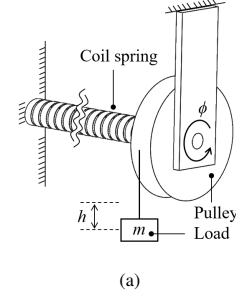


Fig. A1. Strain energy stored by the twist of the coil spring. The strain energy estimated is accorded to the experimental result obtained from the change in the potential energy.

The energy U_s equals to the strain energy derived in (4).

Let us confirm the relation between the strain energy and the angular displacement experimentally. Fig. A1(a) shows the experimental setup. One end of the coil spring is fixed and the other free end is attached to a pulley. The coil spring has a diameter of 11 mm and a wire total length of 310 mm. A weight is loaded to the string connected to the pulley that fixes the free end. When a weight is applied, it moves downwards due to gravity and twists the coil spring with an angular displacement ϕ circumferentially. In this case, the strain energy stored by the twist is equal to the work done by the displacement of the weight. It is described as a half of the potential energy of the weight m and the change in height h :

$$U_p = \frac{1}{2} mgh \quad (A4)$$

This value should take the same value as the strain energies in (A3).

Fig. A1(b) shows the experimental behavior of U_s and U_p when ϕ and h are determined. The plots obtained in the change in the displacement of the mass are in good agreement with the curve of the strain energy. This fact means that the strain energy computed by (4) and (A3) is correct.

REFERENCES

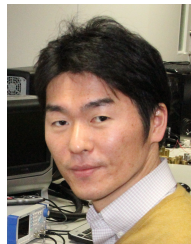
- [1] J. Burgner-Kahrs, D. C. Rucker, and H. Chose, "Continuum robots for medical applications: A survey," *IEEE Trans. Robot.*, vol. 31, no. 6, pp. 1261–1280, 2015.
- [2] D. Trivedi, C. D. Rahn, W. M. Kier, and I. D. Walker, "Soft robotics: Biological inspiration, state of the art, and future research," *Appl. Bionics. Biomechan.*, vol. 5, no. 3, pp. 99–117, 2008.
- [3] S. Kim, C. Laschi, and B. Trimmer, "Soft robotics: A bioinspired evolution in robotics," *Trends Biotechnol.*, vol. 31, no. 5, pp. 287–294, 2013.

- [4] H. B. Gilbert, D. C. Rucker, and R. J. Webster III, "Concentric tube robots: The state of the art and future directions," in *Proc. Int. Sym. Robot. Res.*, 2016, pp. 253–269.
- [5] G. Chen, M. T. Pham, and T. Redarce, "A guidance control strategy for Semi-autonomous colonoscopy using a continuum robot," in *Proc. Int. Conf. Adv. Robot.*, 2008, pp. 63–78.
- [6] M. A. Robertson and J. Paik, "New soft robots really suck: Vacuum-powered systems empower diverse capabilities," *Sci. Robot.*, vol. 2, no. 9, 2017.
- [7] J. Jayender, M. Azizian, and R. V. Patel, "Autonomous image-guided robot-assisted active catheter insertion," *IEEE Trans. Robot.*, vol. 24, no. 4, pp. 858–871, 2008.
- [8] E. Ayvali, C. P. Liang, M. Ho, Y. Chen, and J. P. Desai, "Towards a discretely actuated steerable cannula for diagnostic and therapeutic procedures," *Int. J. Robot. Res.*, vol. 31, no. 5, pp. 588–603, 2012.
- [9] J. H. Crews and G. D. Buckner, "Design optimization of a shape memory alloy-actuated robotic catheter," *J. Intell. Master. Syst. Structures*, vol. 23, no. 5, pp. 545–562, 2012.
- [10] M. D. M. Kutzer, S. M. Segreti, C. Y. Brown, M. Armard, R. H. Taylor, and S. C. Mears, "Design of a new cable-driven manipulator with a large open lumen: Preliminary applications in the minimally-invasive removal of osteolysis," in *Proc. IEEE Conf. Robot. Autom.*, 2011, pp. 2913–2920.
- [11] H. S. Yoon and B. J. Yi, "A 4-DOF flexible continuum robot using a spring backbone," in *Proc. IEEE Int. Conf. Mechatron. Autom.*, 2009, pp. 1249–1254.
- [12] P. Qi, C. Qiu, H. Liu, J. S. Dai, L. D. Seneviratne, and K. Althoefer, "A novel continuum manipulator design using serially connected double-layer planar springs," *IEEE/ASME Trans. Mech.*, vol. 21, no. 3, pp. 1281–1292, 2015.
- [13] K. Zhang, C. Qiu, and J. S. Dai, "An extensible continuum robot with integrated origami parallel modules," *J. Mech. Robot.*, vol. 8, no. 3, 2015.
- [14] E. W. Hawkes, L. H. Blumenschein, J. D. Greer, and A. M. Okamura, "A soft robot that navigates its environment through growth," *Sci. Robot.*, vol. 2, no. 8, 2017.
- [15] S. Ueha, Y. Tomikawa, M. Kurosawa, and N. Nakamura, "Ultrasonic motors: Theory and Applications," *Oxford Clarendon Press*, 1993.
- [16] T. Sashida and T. Kenjo, "An Introduction to Ultrasonic Motors," *Clarendon, Oxford, U.K.*, 1993.
- [17] K. Uchino, "Piezoelectric ultrasonic motors: overview," *Smart Mater. Struct.*, vol. 7, no. 3, pp. 273–285, 1998.
- [18] T. Hemsell and J. Wallaschek, "Survey of the present state of the art of piezoelectric linear motors," *Ultrasonics*, vol. 38, no. 1–8, pp. 37–40, 2000.
- [19] Y. Peng, Y. Peng, X. Gu, J. Wang and H. Yu, "A review of long range piezoelectric motors using frequency leveraged method," *Sens. Actuators A, Phys.*, vol. 235, pp. 240–255, 2015.
- [20] A. Kanada and T. Mashimo, "Flexible Ultrasonic Motor using an output coil spring slider," in *Proc. IEEE/RSJ Int. Conf. Intell. Robots. Syst.*, 2017, pp. 5616–5621.
- [21] T. Mashimo and S. Toyama, "Vibration analysis of cubic rotary-linear piezoelectric actuator," *IEEE Tran. Ultrason. Ferroelectr. Freq. Control*, vol. 58, no. 4, pp. 844–848, 2011.
- [22] T. Funakubo, T. Tsubata, Y. Taniguchi, K. kumei, T. Fujimura, and C. Abe, "Ultrasonic linear motor using multilayer piezoelectric actuators," *Jpn. J. Appl. Phys.*, vol. 34, no. 1, pp. 2756–2759, 1995.
- [23] S. P. Timoshenko, *History of Strength of Materials*, New York: McGraw-Hill, 1953.
- [24] K. Nakamura, M. Kurosawa, H. Kurebayashi, and S. Ueha, "An estimation of load characteristics of an ultrasonic motor by measuring transient responses," *IEEE Trans. Ultrason. Ferroelectr. Freq. Control*, vol. 38, no. 5, pp. 481–485, 1991.
- [25] A. M. Flynn, "Piezoelectric ultrasonic micromotors," *PhD Thesis. Massachusetts Institute of Technology*, 1995.
- [26] T. Mashimo and K. Terashima, "Dynamic Analysis of an Ultrasonic Motor Using Point Contact Model," *Sens. Actuators A, Phys.*, vol. 233, no. 1, pp. 15–21, 1991.
- [27] J. Wu, Y. Mizuno, and K. Nakamura, "Polymer-based ultrasonic motor utilizing high-order vibration modes," *IEEE/ASME Trans. Mechatron.*, vol. 23, no. 2, pp. 788–799, 2018.
- [28] T. Mashimo and S. Toyama, "Rotary-Linear Piezoelectric Microactuator with a Cubic Stator of Side Length 3.5mm," *IEEE Trans. Ultrason. Ferroelectr. Freq. Control*, vol. 57, no. 8, pp. 1825–1830, 2010.



Ayato Kanada received the B.S. and M.S. degrees in mechanical engineering from Toyohashi University of Technology, Japan, in 2015 and 2017, respectively. He is currently working toward the Ph.D. degree at Toyohashi University of Technology.

His research interests are soft actuators and bio mimetic robotics.



Tomoaki Mashimo (M'06) received the Ph.D. degree in mechanical engineering from the Tokyo University of Agriculture and Technology, Fuchu, Japan, in 2008. He was a Robotics Researcher at the Robotics Institute, Carnegie Mellon University, Pittsburgh, PA, USA, from 2008 to 2010. After being an Assistant Professor (tenure-track) with Toyohashi University of Technology, Toyohashi, Japan, in 2011, he became an Associate Professor in 2016. His research interests include piezoelectric actuators and the robotic applications.